Weak-coupling theory for La_2CuO_4

I. E. Dzyaloshinskiĭ and V. M. Yakovenko

L. D. Landau Institute of Theoretical Physics of the USSR Academy of Sciences
(Submitted 26 November 1987)
Zh. Eksp. Teor. Fiz. **94**, 344–355 (April 1988)

Numerical calculations based on the weak coupling theory are carried out for La_2CuO_4.[1,2] The main result is that there is a considerable difference between the Hubbard model with a single charge and the interaction of a general form with four effective charges. In the first case the metal is always unstable and, depending on the sign of the charge, it goes over either to the antiferromagnetic or the superconducting state. In the general case the metal may remain stable or go over to the state, considered previously, consisting of a "singlet superconductivity (SS) + spin density wave (SDW) + charge density wave (CDW)" coherent mixture. Paired SS + CDW, SS + SDW, and SDW + CDW coherent mixtures should also be possible.

1. INTRODUCTION

The present article completes the construction undertaken earlier[1,2] of a weak-coupling theory for La_2CuO_4. This theory is based on the peculiarity of the electronic spectrum of La_2CuO_4 first considered by Hirsch and Scalapino[3] (see also Ref. 4). Naturally, the question arises at once, what is the meaning of weak-coupling limit in a situation when the interaction is clearly of order unity, and possibly even stronger. We believe that the results; for small charges will allow a judicious extrapolation (for more detail, see the Conclusion) into the region of intermediate and strong interaction, where all the qualitative results of the theory remain valid: increase in transition temperatures, the uniqueness of the long-range order and flucutations, etc.

The results of studies of a two-dimensional metal with a nearest-neighbors approximation for the electronic spectrum[1-4] give a basis for such hopes. In this approximation the Fermi surface of La_2CuO_4 is nearly the square shown in Fig. 1a (Refs. 3,4). The existence of the corners leads to an anomalously strong enhancement, proportional to the square of the logarithm of the energy (or temperature), of flucutations of all the possible types of long-range order: singlet superconductivity (SS), spin-density waves (SDW) and charge-density waves (CDW). The strong fluctuations on the one hand lead to a transition temperature different from the BCS formula[3]: $T_c \propto \exp(-\text{const}\, g^{-1/2})$; on the other hand, they in general render useless simple ladder theories of the BCS type.[1,2] The behavior of the system is determined by complicated nonlinear integrodifferential equations describing the coexisting of strong fluctuations of all three types. These equations can only be solved numerically.

The SS, SDW and CDW interaction is most clearly manifested in the dependence of the state of the material on the bare charges. In the weak-coupling approximation there are four charges in all.[1,2] In the Hubbard limit, when all the charges are equal and positive, the results of numerical calculation (Sec. 3) are practically the same as those of the ladder approximation[2,3]: the system is antiferromagnetic and is in an almost pure SDW state. (Note that in the nonphysical variant of the Hubbard model with attraction the system would be in the SS + SDW state given by the ladder approximation: a metal is always unstable in the Hubbard model.)

In the general case of different bare charges, the picture given by numerical calculation is unexpectedly rich. On the one hand, there is the region of metallic stability and on the other, there is the possibility discussed earlier[1,2] of a monster—a coherent combination of SS + SDW + CDW. By symmetry considerations[2] this monster is necessarily ferromagnetic, which unexpectedly conflicts with the old results of Nagaoka[5] in the strong-coupling limit.

Finally, even at first glance, the pure SS, SDW or CDW states for unequal bare charges differ noticeably from the results of the ladder approximation. Besides the leading fluctuations (for example, SDW) there is a distinct admixture of the other functions (SS and CDW) which, in its turn, distorts the pure state, leading to an intrinsic dependence of the renormalized charges on electron momentum.

The results of numerical calculation are described in detail in Sec. 3. In addition, we have outlined the calculational method (Sec. 2).

2. CALCULATIONAL METHOD

We first simplify somewhat the system (9) of parquet equations in Ref. 2. From symmetry considerations for identical particles it follows that in Eq. (7) of Ref. 2

$$\gamma_1=\gamma_{-1}, \quad \gamma_2=\gamma_{-2}. \tag{1}$$

In addition, the diagrams for γ_1 can be cut off at the Cooper diagrams, and for γ_3 and γ_4, at the zero-sound diagrams, that is,

$$\gamma_1=g_1+C_1, \quad \gamma_3=g_3+Z_3, \quad \gamma_4=g_4+Z_4, \quad \gamma_2=g_2+C+Z_I+Z_{II}. \tag{2}$$

Thus, we have six unknown functions in all, γ_1, γ_3, γ_4, C, Z_I and Z_{II}, which must be determined by solution of the parquet equations.

Each of these quantities is a function of four variables. A natural choice of these variables for the functions considered is listed below [the notation is from Eq. (8) of Ref. 2]:

$$\begin{aligned} &\gamma_1(\xi_1, \xi_2(c), \eta_1, \eta_3), \quad \gamma_3(\xi_1, \xi_2(z), \eta_1, \eta_2), \\ &\gamma_4(\xi_1, \xi_2(\bar{z}), \eta_1, \eta_2), \quad C(\xi_1, \xi_2(c), \eta_1, \eta_3), \\ &Z_I(\xi_1, \xi_2(z), \eta_1, \eta_2), \quad Z_{II}(\xi_1, \xi_2(\bar{z}), \eta_1, \eta_2). \end{aligned} \tag{3}$$

From a formal mathematical point of view, the arguments of all the functions (3) can be denoted in an arbitrary way, for example $(\xi_1, \xi_2, \zeta_1, \zeta_2)$. It is understood that for each of the functions $\gamma_1, \gamma_3, \gamma_4, C, Z_I$ and Z_{II} these arguments have their

 0038-5646/88/040844-06$04.00

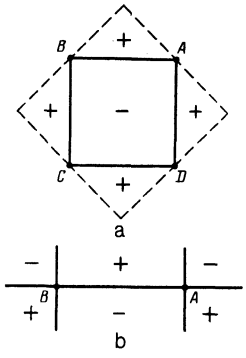

FIG. 1.

own physical meaning, determined according to (3) and Eq. (8) in Ref. 2. Furthermore, we will employ this same notation for the arguments of all the functions (3).

To simplify the notation, we introduce the following symbol. Let A, B, C be arbitrary functions of four variables $(\xi_1, \xi_2, \zeta_1, \zeta_2)$. Then we will write an expression of the form

$$\frac{d}{d\xi_1} A(\xi_1, \xi_2, \zeta_1, \zeta_2) = \int_0^{\xi_2} d\zeta\, B(\xi_1, \xi_2, \zeta_1, \zeta) C(\xi_1, \xi_2, \zeta, \zeta_2) \tag{4}$$

as the convolution

$$A = B \circ C. \tag{5}$$

For the arbitrary function $A(\xi_1, \xi_2, \zeta_1, \zeta_2)$ we introduce the function $\tilde{A}(\xi_1, \xi_2, \zeta_1, \zeta_2)$ of four variables, which is connected with the original function by the following relation:

$$\tilde{A}(\xi_1, \xi_2, \zeta_1, \zeta_2) = A(\xi_1, \min(\zeta_1, \zeta_2), \min(\zeta_1, \zeta_2), \min(\zeta_1, \zeta_2)). \tag{6}$$

Then, in the notation of (5) and (6), the parquet equations for the functions (3) take the form

$$\begin{aligned}
\dot{\gamma}_1 &= -\gamma_1 \circ \gamma_1 - \gamma_{III} \circ \gamma_{III}, \\
\dot{\gamma}_3 &= -2\gamma_{II} \circ \gamma_{II} + \gamma_{II} \circ \gamma_1 + \gamma_1 \circ \gamma_{II} - 2\gamma_3 \circ \gamma_3 + \gamma_3 \circ \gamma_4 + \gamma_4 \circ \gamma_3, \\
\dot{\gamma}_4 &= \gamma_4 \circ \gamma_4 + \gamma_I \circ \gamma_I, \\
\dot{C} &= -\gamma_1 \circ \gamma_{III} - \gamma_{III} \circ \gamma_1, \\
\dot{Z}_I &= \gamma_I \circ \gamma_4 + \gamma_4 \circ \gamma_I, \\
\dot{Z}_{II} &= \gamma_{II} \circ (\gamma_4 - 2\gamma_3) + (\gamma_4 - 2\gamma_3) \circ \gamma_{II} + \gamma_1 \circ \gamma_3 + \gamma_3 \circ \gamma_1,
\end{aligned} \tag{7}$$

where

$$\begin{aligned}
\gamma_I &= g_2 + Z_I + \tilde{Z}_{II} + \tilde{C}, \quad \gamma_{II} = g_2 + Z_{II} + \tilde{Z}_I + \tilde{C}, \\
\gamma_{III} &= g_2 + C + \tilde{Z}_I + \tilde{Z}_{II}.
\end{aligned} \tag{8}$$

The quantities γ_I, γ_{II}, γ_{III} in (8) are just the vertex γ_2, written in terms of the different sets of arguments (8) of Ref. 2. The different combinations of "tilde" signs over Z_I, Z_{II} and C appear in passing from one set of arguments to another with logarithmic accuracy.[6]

The Eqs. (7) and (8) were solved numerically. For this, expression (4) was replaced by its discrete analog. The vertices γ, C, Z were calculated in the form nD, where $0 \leqslant n \leqslant 16$ is an integer, and $D = 1/16$ is the mesh interval. The interval on the right side of (4) was replaced by a summation using the trapezoid rule. For $A(\xi_1, \xi_2, \zeta_1, \zeta_2) = A(\xi_1, \xi_2, \zeta_2, \zeta_1)$ and $\xi_2 \geqslant \zeta_1, \zeta_2$, it is sufficient to consider the range of arguments $\xi_2 \geqslant \zeta_1 \geqslant \zeta_2$. Thus from the system (7) we get the system consisting of

$$6 \sum_{k=0}^{16} \sum_{l=0}^{k} \sum_{m=0}^{l} 1 = 5814$$

ordinary differential equations in the variable ξ_1, taken to be time. This system of 5814 equations was solved numerically by the fourth-order Runge-Kutta method with initial conditions, at $\xi_1 = 0$, of:

$$\gamma_1 = g_1, \quad \gamma_3 = g_3, \quad \gamma_4 = g_4, \quad C = Z_I = Z_{II} = 0. \tag{9}$$

Results of the numerical solution are discussed in Sec. 3; here we transform (7) and (8) into another form more convenient for analytical investigation and interpretation of the numerical results.

Solving Eqs. (7) by iteration in time ξ_1, we see easily that for any of the functions γ_1, γ_3, γ_4, C, Z_I, Z_{II} we get an expansion of the form

$$A(\xi_1, \xi_2, \zeta_1, \zeta_2) = \sum_{klmnpq} a_{k,l,m,n,p,q} g_1^{n-m-p-q} g_2^m g_3^p g_4^q \xi_1^n \xi_2^{-k-l} \zeta_1^k \zeta_2^l. \tag{10}$$

This implies that the function $A(\xi_1, \xi_2, \zeta_1 \zeta_2)$ is in fact a function of three arguments: $\xi_1 \xi_2 = \theta$, $\zeta_1/\zeta_2 = X$, and $\zeta_2/\xi_2 = Y$:

$$\begin{aligned}
A(\xi_1, \xi_2, \zeta_1, \zeta_2) &= A'(\xi_1 \xi_2, \zeta_1/\xi_2, \zeta_2/\xi_2) \\
&= A'(\theta, X, Y), \quad 0 \leqslant X \leqslant 1, \quad 0 \leqslant Y \leqslant 1.
\end{aligned} \tag{11}$$

If we consider each of the quantities γ_1, γ_3, γ_4, C, Z_I, Z_{II} as a function if θ, X, and Y, then the parquet equations for these functions will have the form of (7) and (8), where now the derivative and the convolution (5) are expressed as

$$\frac{d}{d\theta} A(\theta, X, Y) = \int_0^1 dZ\, B(\theta, X, Z) C(\theta, Z, Y), \tag{12}$$

and, in place of (6), we have

$$\tilde{A}(\theta, X, Y) = A(\theta \min(X, Y), 1, 1). \tag{13}$$

Note that the terms with a tilde entering into (8) are, according to (13), retarded in time with respect to the terms without the tilde. Therefore, according to (7) and (8), the derivatives $\dot{A}(\theta, X, Y)$ depend not only on the values of the functions $A(\theta, X, Y)$ at that same instant θ of time, but on their values at preceding times. In other words, the system of Eqs. (7), (8), (5), (12) and (13) is a system of differential equations with a memory.

Numerical results from the formulation (4) and (6) become more transparent in the retarded representation of (12) and (13). In Figs. 2, 3, 4 and 6, different functions $A(\theta, X, Y)$ for fixed θ are contained in the XY plane. On each plot 11 conton-S are drawn, with the interval (MAX–MIN)/12, where

$$\mathrm{MAX}=\max_{X,Y}[A(\theta,X,Y)],\qquad \mathrm{MIN}=\min_{X,Y}[A(\theta,X,Y)].$$

Cross-hatches indicate the direction of decrease. In the captions the values of θ, MAX and MIN are shown.

We now transform the system of Eqs. (7) and (8) to a simpler form. We introduce the quantities

$$\gamma_{a,\pm}=-\gamma_1\pm C,\quad \gamma_{b,\pm}=\gamma_4\pm Z_{\mathrm{I}},$$
$$\gamma_{c,\pm}=\gamma_4-2\gamma_3\mp(Z_{\mathrm{I}}-2Z_{\mathrm{II}}). \tag{14}$$

Equations (7) and (8), written in terms of the variables (14), have the form

$$\dot\gamma_{a,\pm}=\{\gamma_{a,\pm}\pm[g_2+{}^3/_4(\tilde\gamma_{b,+}-\tilde\gamma_{b,-})+{}^1/_4(\tilde\gamma_{c,+}-\tilde\gamma_{c,-})]\}^2,$$
$$\dot\gamma_{b,\pm}=\{\gamma_{b,\pm}\pm[g_2+{}^1/_2(\tilde\gamma_{a,+}-\tilde\gamma_{a,-})+{}^1/_4(\tilde\gamma_{b,+}-\tilde\gamma_{b,-})$$
$$+{}^1/_4(\tilde\gamma_{c,+}-\tilde\gamma_{c,-})]\}^2, \tag{15}$$
$$\dot\gamma_{c,\pm}=\{\gamma_{c,\pm}\pm[g_2+{}^1/_2(\tilde\gamma_{a,+}-\tilde\gamma_{a,-})+{}^3/_2(\tilde\gamma_{b,+}$$
$$-\tilde\gamma_{b,-})-{}^1/_4(\gamma_{c,+}-\tilde\gamma_{c,-})]\}^2,$$

where the notation $A^2=A\circ A$ is used in the sense of (5). The initial conditions (9) now take the form

$$\gamma_{a,+}=\gamma_{a,-}=-g_1,\quad \gamma_{b,+}=\gamma_{b,-}=g_4,\quad \gamma_{c,+}=\gamma_{c,-}=g_4-2g_3. \tag{16}$$

If we discard the retarded terms in Eqs. (15), then these equations decouple and coincide with the equations of the ladder approximation. Thus, the whole parquet effect lies in the existence of the time-retarded terms in (15), which link these equations.

Having solved Eqs. (15) [or the equivalent Eqs. (7) and (8)] we can find the susceptibilities $\chi_i(\theta)$ corresponding to the different types of electronic instabilities in the system. In the model considered there are six types of instabilities: $\mathrm{SS}^\pm$, $\mathrm{SDW}^\pm$, and $\mathrm{CDW}^\pm$. The $\pm$ signs correspond to order parameters that are symmetric or antisymmetric with respect to interchange of the van Hove points A and B in Fig. 1b. In the case of a + sign(− sign) and s-type (d-type) pairing takes place, for which the order parameter does not change sign (changes sign twice) on traversing the square Fermi surface.

To find $\chi_i(\theta)$, we must first calculate the auxiliary quantity $\mathcal{T}_i(\theta,X)$, making use of the equation

$$\frac{d}{d\theta}\mathcal{T}_i(\theta,X)=\int_0^1 dY\,\Gamma_i(\theta,X,Y)\mathcal{T}_i(\theta,Y),$$
$$i=\mathrm{SS}^\pm,\ \mathrm{SDW}^\pm,\ \mathrm{CDW}^\pm \tag{17}$$

where $\Gamma_i(\theta,X,Y)$ coincides with the expressions in curly brackets in (15), and the following correspondence exists between the indices in (17) and (15):

$$a,\pm\leftrightarrow\mathrm{SS}^\mp,\quad b,\pm\leftrightarrow\mathrm{SDW}^\pm,\quad c,\pm\leftrightarrow\mathrm{CDW}^\mp. \tag{18}$$

In terms of the original variables of (2) and (8) the Γ_i have the following form:

$$\Gamma_{\mathrm{SS}^\pm}=-\gamma_1\mp\gamma_{\mathrm{III}},\quad \Gamma_{\mathrm{SDW}^\pm}=\gamma_4\pm\gamma_{\mathrm{I}},$$
$$\Gamma_{\mathrm{CDW}^\pm}=\gamma_4-2\gamma_3\pm(\gamma_{\mathrm{I}}-2\gamma_{\mathrm{II}}). \tag{19}$$

Taking account of the correspondence (18) and Eqs. (14) and (15), the quantities $\gamma_{a,\pm}$, $\gamma_{b,\pm}$, $\gamma_{c,\pm}$, differ from (19) only by the absence of the retarded terms and the constant g_2. Then we have

$$\chi_i(\theta)=\int_0^1 dX\,\mathcal{T}_i^2(\theta,X). \tag{20}$$

All this procedure was carried out numerically.

3. RESULTS OF THE NUMERICAL CALCULATION

The results of the numerical calculation are collected in the table. The quantity θ_s in the table is the time for which the solution of the system of Eqs. (7) becomes singular. It is related to the transition temperature by the formula

$$T_c=\mathrm{const}\cdot\exp\{-(\theta_s/|g|)^{1/2}\},$$

where $|g|$ is the general scale constant g_1,g_2,g_3,g_4 (the calculational results are valid, of course, for sets of g_1,g_2,g_3,g_4 differing by an overall multiplying factor $|g|$). The quantity θ_l is the estimate for θ_s in the ladder approximation. The row designated by χ indicates which of the susceptibilities $\chi_i\to\infty$ for $\theta\to\theta_s$. We note that in all the cases investigated the form of the instability agrees with that given by the ladder approximation. Below, we comment on the most typical solutions.

a) The Hubbard model, $g_1=g_2=g_3=g_4$. As was already said, the results in rough outline differ little from the ladder results of Ref. 2 [Eqs. (13)–(15)]. The transition point is fixed by the value $\theta_s=0.52$ (the ladder would give $\theta_l=0.50$). For $g>0$ the leading instability, naturally, turns out to be the SDW^+, and the leading renormalized charge γ_4 as a function of the relative momenta X and Y changes by less than 15% (Fig. 2a). However, the "strange" vertices depend very strongly on the momenta. In Fig. 2b the isolines of γ_1 are shown for $\theta=0.52$. It is evident that as the transition point is approached the charge γ_1, initially positive, takes a negative "superconducting" sign. Moreover, the superconducting region arises from the region of momenta near the

TABLE I.

No. of conditions	1	2	3	4	5	6	7
g_1	1	−1	−0.5	1	1	1	1
g_2	1	−1	−1	2	2	0.5	1
g_3	1	−1	−1	0	0.5	0	0
g_4	1	−1	−1	−1	−1.5	−1	−1
χ	SDW^+	SS^+, CDW^+	CDW^+	SS^-, SDW^+, CDW^-	SS^-	—	—
θ_s	0.52	0.52	0.56	2.2	5.3	>2.1	>12.5
θ_l	0.5	0.5	0.5	1.0	1.0	—	—

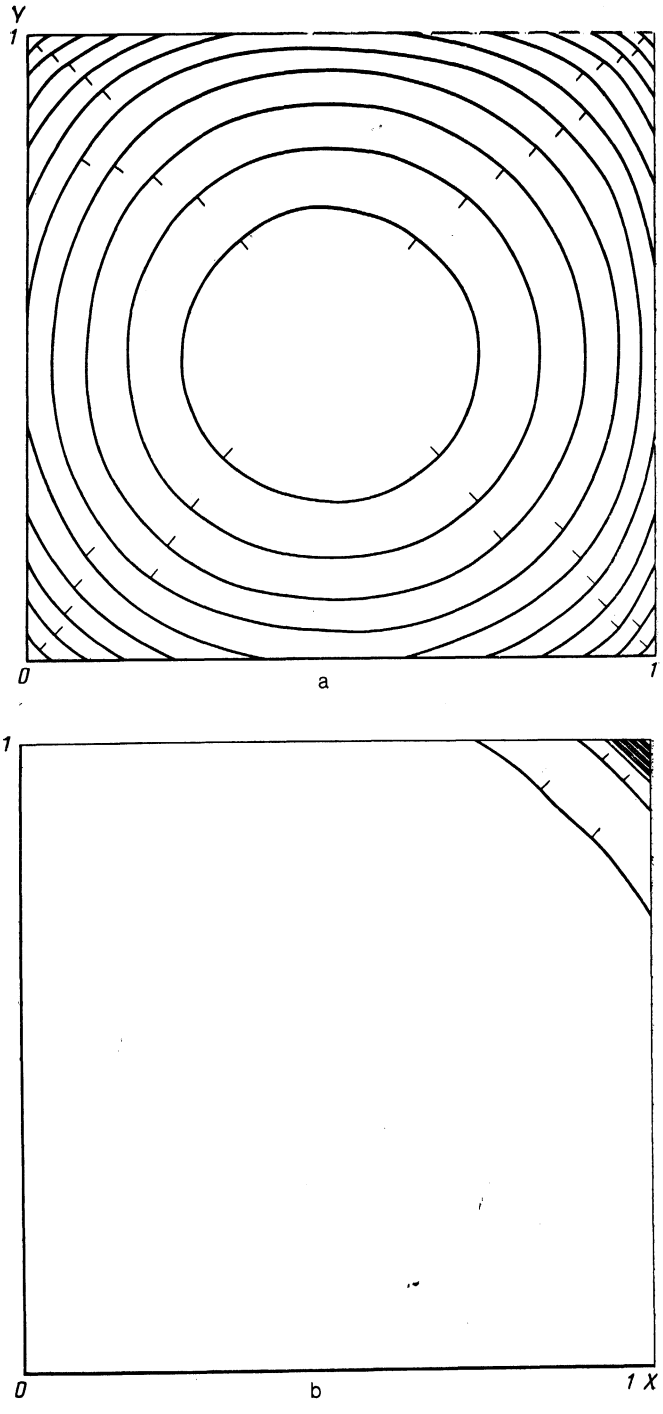

FIG. 2. Contours of the function $A(\theta,X,Y)$ for initial conditions No. 1 and $\theta = 0.52$: a—$\gamma_4(\theta,X,Y)$, MAX = 379, MIN = 331, b—$\gamma_1(\theta,X,Y)$, MAX = 0.5, MIN = -14.8.

points A and B in Fig. 1b (the upper right-hand corner $X = Y = 1$, Fig. 2b), as far as possilbe from the region of perturbation theory (the coordinate origin).

This behavior can be understood as follows. Neglecting the retarded terms in Eq. (15) for $\gamma_{b,+}$, for θ near θ_s we get the equation

$$\dot{\gamma}_{b,+} = (\gamma_{b,+} + g_2)^2,$$

which has a solution of the form

$$\gamma_{b,+}(\theta, X, Y) + g_2 = \text{const}/(\theta_s - \theta). \quad (21)$$

Substituting the expression in the remaining equations of (15), we find, for example, that

$$\gamma_{a,+}(\theta, X, X) \sim \ln(\theta_s - \theta + 1 - X). \quad (22)$$

We see that a pole in the SDW channel leads to the appearance of only a weak logarithmic singularity in other channels, and only at points near $X = Y = 1$. Thus the neglect of the retarded terms is valid.

The Hubbard model preserves the symmetry, relative to changes of sign in charge, inherent in the ladder approximation. for $g < 0$ the driving instabilities are the SS^+ and CDW^+, and Fig. 2b depicts (with the opposite sign) the isolines for γ_4.

For interactions of general character with differing bare charges the stability region for the different types $SS^\pm$, $SDW^\pm$, and $CDW^\pm$ is roughly determined by the ladder Eqs. (13)–(15) in Ref. 2 for the transition points. We begin with the most interesting charge regime, where the SS, SDW and CDW coexist.

b) $g_1 = 1$, $g_2 = 2$, $g_3 = 0$, $g_4 = -1$. In the ladder approximation we have a $SS^- + SDW^+ + CDW^-$ instability for these values of charges, approaching $\theta_l = 1.0$. This same coherent mixture remains unstable in the parquet approximation although the transition temperature is lower: $\theta_s = 2.2$. The unsuitability of the ladder approximation appears more vividly in the sharp dependence of the vertices on momenta. The leading renormalized charge has a characteristic peak for large momenta (that is, for $X = Y = 0$), and the charge $\gamma_{a,-} = \gamma_{b,-} = \gamma_{c,-}$ turns out to be a nontrivial function of the momenta, having maxima for $X = Y = 0$ and $X = Y = 1$ (Fig. 3b).

In the ladder approximation the coherent mixture SS + SDW + CDW is unstable. If one moves away from the point at which the bare charges g_{SS^-}, g_{SDW^+} and g_{CDW^-} are equal, there will be one leading channel, an the other two become unfavorable. In the parquet approximation the situation is not so fixed. An appraisal taking into account the dependence of the renormalized charges on the momenta shows that, apparently, there is a final region of instability that is a SS + SDW + CDW monster.

This means that even when one channel clearly dominates, the results are none the less far from those of the ladder approximation. We will describe one of these symmetric situations.

c) $g_1 = 1$, $g_2 = 2$, $g_3 = 0.5$, $g_4 = -1.5$. In the ladder approximation a SS^- instability develops for $\theta_l = 1.0$. The SS^- instability remains the sole driving instability in the parquet approximation, but the transition temperature differs greatly: $\theta_s = 5.3$. The momentum dependence of the renormalized charge is nontrivial. The leading charge $\gamma_{a,+}$ again has a sharp peak for large momenta ($X = Y = 0$) and the charge γ_4 alternates as a function of X and Y in sign (Fig. 4).

Finally, on the metallic instability: in the ladder approximation the region of metallic instability always exists (see Eqs. (13)–(15) in Ref. 2). We cite the results on the boundary of the instability in the ladder approximation:

$$g_{SS^-} = g_{SDW^+} = g_{CDW^-} = 0.$$

d) $g_1 = g_2 = 1$, $g_3 = 0$, $g_4 = -1$. Here at first glance we have the zero-charge picture, which we traced up to the

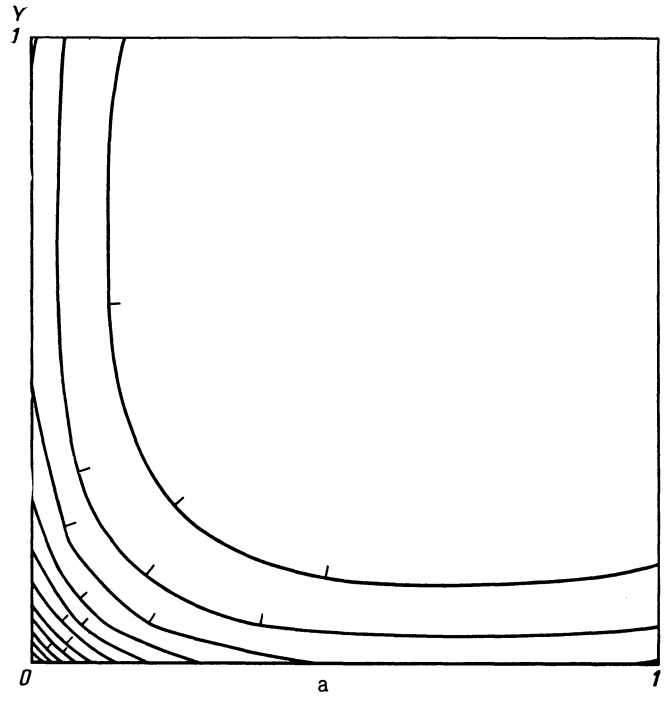

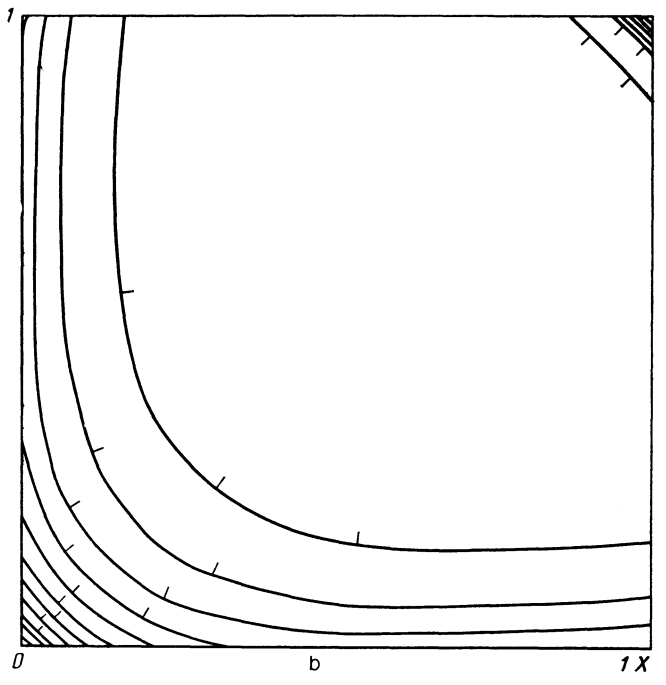

FIG. 3. Contours of the function $A(\theta,X,Y)$ for initial conditions No. 4 and $\theta = 2.1$: a—$\gamma_{a,+}(\theta,X,Y)$, MAX = 528, MIN = 46; b—$\gamma_{a,-}(\theta,X,Y)$, MAX = 2.4, MIN = 0.7.

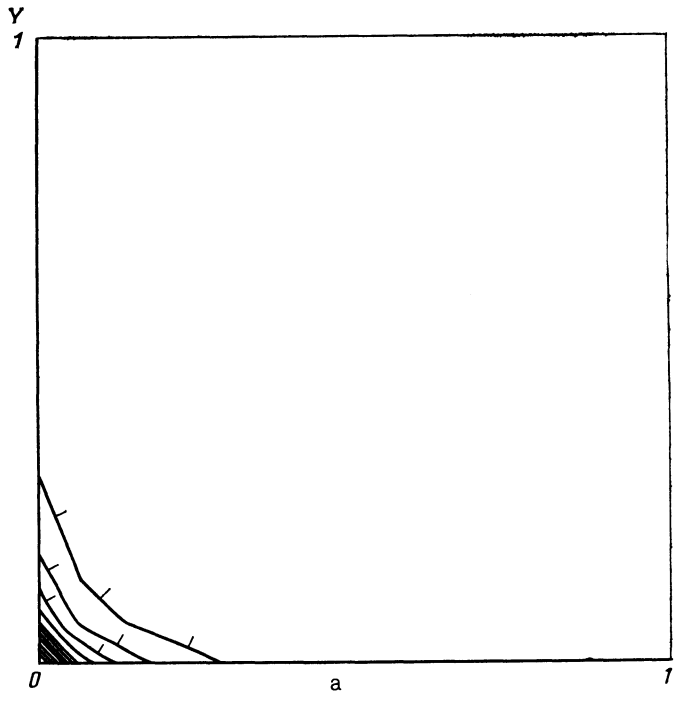

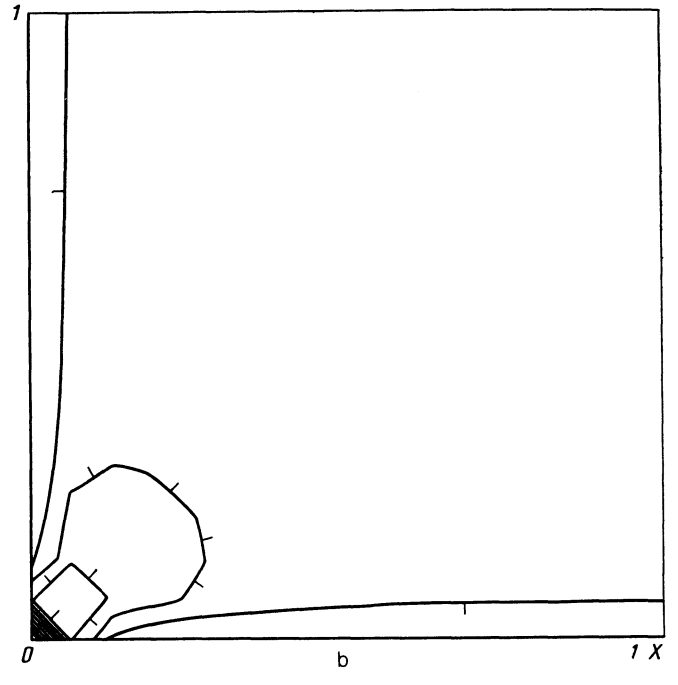

FIG. 4. Contours of the function $A(\theta,X,Y)$ for initial conditions No. 5 and $\theta = 5.2$: a—$\gamma_{a,+}$,(θ,X,Y), MAX = 2596, MIN = -0.3; b—$\gamma_4(\theta,X,Y)$, MAX = 2.3, MIN = -0.5.

value $\theta = 12.5$. The generalized susceptibilities $\chi_{SS^-} = \chi_{SDW^+} = \chi_{CDW^-}$ in the region $\theta > 3$ depend linearly on θ, which corresponds to all the $\Gamma_i \to 0$ according to (17) and (20) (Fig. 5). However, the renormalized charges $\Gamma_{SS^-} = \Gamma_{SDW^+} = \Gamma_{CDW^-}$ are still intrinsic functions of the momenta, on the order of unity, and only their alternating character leads to the vanishing of the integrals determining the susceptibility. It is difficult to visualize how such precise cancellation remains right up to $\theta = \infty$ ($T = 0$). A more likely picture is that for some—possibly very large—value of θ the compensation breaks down and the system suddenly undergoes a phase transition.

In Fig. 6, as illustration, the values of $\gamma_{a,-}$ are shown for $\theta = 7.2$. The remaining vertices have an analogous form. With subsequent evolution in θ they hardly change over the whole XY plane, with the exception of the vicinity of the point $X = Y = 0$. The quantities $\gamma_{a,\pm}$,$\gamma_{b,\pm}$ and $\gamma_{c,\pm}$ tend to constant values of $\mp 1/3$, for which the right-hand sides; of (15) vanish. Since they cease to depend on θ, X and Y, the retarded quantities $\tilde{A}(\theta,X,Y)$ approximately coincide with

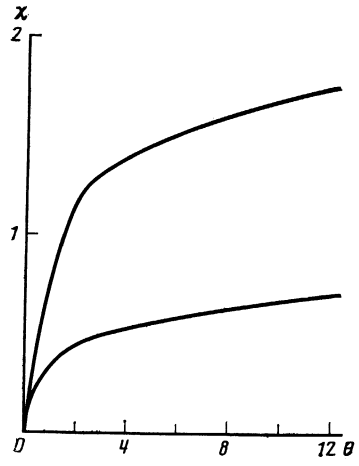

FIG. 5. Behavior of $\chi_{SS^-}(\theta)$ (upper curve) and $\chi_{SS^+}(\theta)$ (lower curve) for initial conditions No. 7.

the $A(\theta,X,Y)$. The exception is in the neighborhood of the point $X = Y = 0$, since there the retarded terms cancel out:

$$\dot{\gamma}_{j,\pm}(\theta,0,0) = \int_0^1 dZ[\gamma_{j,\pm}(\theta,0,Z) \pm g_2]^2 \qquad j=a,b,c. \qquad (23)$$

We see that the right side of (23) is positive and roughly equal to $(2/3)^2$. Thus at the point $X = Y = 0$ there is a linear increase with time. It is very likely that it turns into a polar singularity at the point $X = Y = 0$. In fact, just such an instability arose in cases (b) and (c) studied above.

The results presented demonstrate the richness of the weak-coupling model with four bare charges. Particularly instructive is the possibility of a coherent combination of all the conceivable types of instabilities (and the corresponding fluctuations). This monster appears in asymmetric situations when the size of the charges is substantially different; at the most extreme g_2 should flip over (see Refs. 1 and 2). In particular, for $|g_2| \to \infty$ the monster is always stable. The charge asymmetry automatically implies that the model takes into account interaction with a large number of neighbors; this interaction should in principal be alternating. In this same way the competition between Coulomb repulsion and attraction via phonon exchange is included, allowing one to explain the nontrivial isotope effect in compounds based on La_2Cu_4.

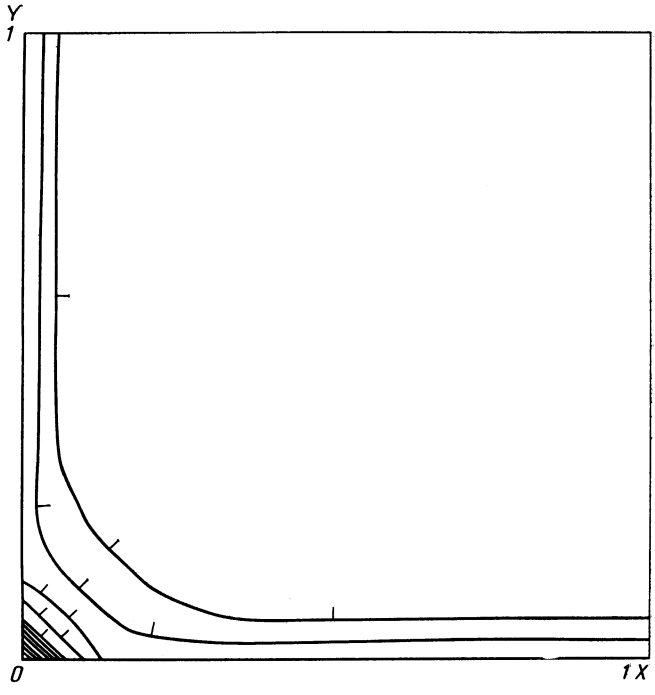

FIG. 6. The quantity $\gamma_{a,-}(\theta,X,Y)$, with $\theta = 7.2$, MAX = 2.0, MIN = 0.2, and initial conditions No. 7.

4. CONCLUSION

In conclusion we turn again to the question of how the weak-coupling model relates to reality. We cannot exclude completely the possibility that in actual La_2CuO_4 and the related compounds we are dealing with moderate or at least not too strong coupling. In this situation the effect of the specific (square) shape of the Fermi surface can be entirely preserved, and then all the consequent features of the model will be manifested. A large number of bare charges allows one to explain simply the experimentally observed sensitivity of La_2CuO_{4-x} to oxygen content. In the weak-coupling limit the effect of alloying, in particular the suppression of antiferromagnetism and the onset of superconductivity, is easily and naturally explained. The theoretical possibility of coherent SS + SDW + CDW mixtures is compatible with the experimental hints of the coexistence of superconductivity, ferromagnetism and antiferromagnetism. Finally, it is not difficult in theory to consider three-dimensional effects as well, putting in interaction between different copper layers.

We intentionally do not cite experimental work, so as not to create the illusion that we have any sort of formula ready for comparison with experiment. In view of its logarithmic accuracy, the theory can give only qualitative results in spite of its complexity. The result of a double-logarithmic approximation would have meaning only for extremely weak coupling.

[1)]These charges are fixed by the value of the corresponding vertices (19) for $\theta = 0$.

[1]I. E. Dzyaloshinskiĭ, Pis'ma v Zh. Eksp. Teor. Fiz. **46**, 110 (Appendix) (1987) [JETP Lett. **46** (1987)].
[2]I. E. Dzyaloshinskiĭ, Zh. Eksp. Teor. Fiz. **93** 1487 (1987) [Sov. Phys.—JETP **66**, 848 (1987)].
[3]J. E. Hirsch and D. J. Scalapino, Phys. Rev. Lett. **56**, 2732 (1986).
[4]J. P. Jorgensen, H. B. Schutter, and D. G. Hinks, Phys. Rev. Lett. **58**, 1024 (1987); L. F. Matheiss, Phys. Rev. Lett. **58**, 1028 (1987).
[5]Y. Nagaoka, Phys. Rev. **147**, 392 (1966).
[6]I. T. Dyatlov, V. V. Sudakov, and K. A. Ter-Martirosyan, Zh. Eksp. Teor. Fiz. **32**, 767 (1957) [Sov. Phys.—JETP **5**, 631 (1957)].

Translated by I. A. Howard